

# Development of Electromagnetic Tomography (EMT) for Industrial Applications. Part 1: Sensor Design and Instrumentation

A J Peyton<sup>1</sup>, M S Beck<sup>2</sup>, A R Borges<sup>3</sup>, J E de Oliveira<sup>3</sup>, G M Lyon<sup>1</sup>, Z Z Yu<sup>1</sup>,  
M W Brown<sup>1</sup>, J Ferrera<sup>3</sup>

<sup>1</sup> Engineering Department, Lancaster University, UK, a.peyton@lancaster.ac.uk

<sup>2</sup> Department of Electrical Engineering and Electronics, UMIST, Manchester, UK

<sup>3</sup> INESC-Aveiro, Portugal, ruib@inesca.inesca.pt

**Abstract** – This paper is the first of two parts and reviews results of a project based at the University of Aveiro, UMIST and the University of Lancaster. This research represents a fundamental investigation of the potential of using electromagnetic inductance measurements for industrial tomographic applications.

This paper concentrates on sensor and instrumentation issues. The systems studied can image the distribution of either electrically conducting material ( $\sigma > 1 \text{ S/m}$ ) and/or magnetically permeable materials ( $\mu_r > 1$ ). The technique has analogies with other forms of electrical tomography such as those based on resistance or capacitance methods. The paper describes the overall operation of an electromagnetic tomography (EMT) system, the design of the sensor array and associated conditioning electronics, and finite element simulation studies on the sensor array with selected results. The system is controlled from an embedded PC and image capture rates are listed. Related topics such as the range of image reconstruction algorithms used, the performance of the systems in terms of image resolution / reconstruction rates and potential industrial applications of the technique are discussed.

**Keywords** : Sensors, Tomography, Electromagnetic, and Inductance.

## 1. INTRODUCTION

There has been considerable international interest shown over the past decade in tomographic imaging techniques and their application to process, industrial and medical problems [1]. Electrical techniques, in particular, are proving very successful in these areas, providing inexpensive non-intrusive imaging systems with low but sufficient resolution of the internal distributions of processes. This paper describes electromagnetic inductance tomography [2-4], which is an electrical tomographic method based on the use of inductance measurements. The technique can generate images based on the distribution of electrically conductive and magnetically permeable material within the object space. The development of EMT together with ECT and ERT provide three fundamental electrical tomography techniques based on the measurement of resistance, capacitance and now inductance, which collectively are able to image the three passive electromagnetic properties of materials.

A brief summary of ECT, ERT and EMT is shown in Table 1.

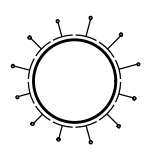
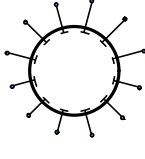
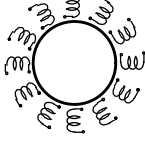
Method	Typical arrangement	Measure values	Typical material properties	Typical material
ECT	 Capacitive plates	Capacitance C	$\epsilon_r$ $10^0 - (10^2)$ $\sigma$ $< 10^{-1} \text{ S/m}$ (low)	Oil, de-ionised water, non-metallic powders, polymers, burning gasses
ERT (EIT)	 Electrode array	Resistance (Impedance) R (Z)	$\sigma$ $10^{-1} - 10^7 \text{ S/m}$ (wide) $\epsilon_r$ $10^0 - 10^2$	Water / saline, biological tissue, rock /geological materials, semi-conductors e.g. silicon
EMT	 Coil array	Self/ mutual Inductance L / M	$\sigma$ $10^2 - 10^7 \text{ S/m}$ (high) $\mu_r$ $10^0 \text{ to } 10^4$	Metals, some minerals, magnetic materials and ionised water

Table 1. Comparison of electrical tomography techniques

Potential applications for EMT techniques are where the material distribution can be characterised by either a high electrical conductivity or ferro- / ferri- magnetic behaviour. Possible examples may include the tracking of ferrite labelled powder in transport / separation processes, foreign body detection and location, food inspection and validation of metal components for defects. Previous research [3] also suggest the possibility of imaging bulk ionised water distributions within equipment, especially pipelines.

## 2. PRINCIPLE OF OPERATION

The principle operation of EMT and the other electrical tomography methods are very similar and can be split into 4 generic operations, namely,

- excitation of the region of interest with an energising field
- distortion of the field contours resulting from the material positioned within the object space.
- boundary measurement of the resulting peripheral field values.
- image reconstruction, often termed the inverse problem, which involves converting the measurements back into an image of the original material distribution.

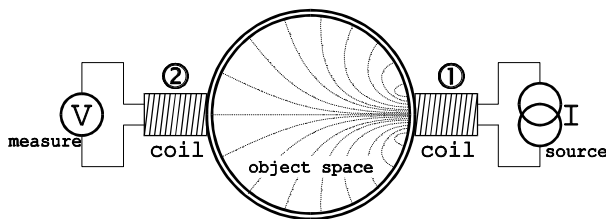


Figure 1. Twin coil EMT example

EMT operates by exciting the region of interest with an AC magnetic field. By comparison ECT, ERT and EIT all use electric field excitation. Referring to the twin coil example shown in Figure 1., a sinusoidal current is passed through coil ① (the energising coil) to generate the magnetic field within the object space. We can assume a background condition with a relative permeability of 1 when the object space is empty (filled with air). In this condition a measurable voltage will be induced across coil ② (the detection coil), corresponding to a background or empty space measurement. The spatial distribution of the magnetic field and hence the mutual coupling between the coils is altered by the introduction of magnetic (relative permeability > 1) and / or metallic (high conductivity) items inside the object space. Magnetic material generally increases the mutual coupling between the coils, resulting in an increased measurement, whereas

conducting objects generally attenuate the measurement due to eddy current losses in the material itself.

A formal description of the instrument system can be derived from Maxwell's equations in complex vector notation as described previously [5]. For a practical two dimensional case (x-y plane), we can make a number of assumptions such as ignoring the effects of the displacement current which may be negligible for the materials and signal frequencies,  $\omega$ , of interest ( $\omega \epsilon \ll s$ ). Free charges can be neglected and the material can be assumed to have linear and isotropic electrical and magnetic properties. Then we have,

$$\nabla \times \left[ \frac{\nabla \times \mathbf{B}_{x,y}}{\mathbf{m}_{x,y}} \right] / \mathbf{s}_{x,y} = -j\omega \mathbf{B}_{x,y} \quad \nabla \cdot \mathbf{B}_{x,y} = 0 \quad (1)$$

where,  $\mathbf{B}$  is the magnetic flux density vector.

The tomographic problem is therefore to excite the object space with a number of spatially distinct field strength profiles, which are loosely termed as projections. For each field profile,  $\mathbf{B}_{x,y}$  can be measured at the boundary of the object space. A sufficient number of projections and field measurements must be used to provide an adequate measurement set to enable images of acceptable quality to be produced. To achieve this objective, the object space is surrounded by an array of coils. To obtain the maximum amount of information from the object space measurements of the real and imaginary components of both the radial and tangential field components should be resolved. However practical systems, to date, ignore the tangential field components often because of the effects of the screening material.

Equation (1) describes the forward problem for EMT. The inverse problem, i.e. image reconstruction, presents formidable difficulties and no complete theoretical solution has yet been devised. In general for electrical tomography the object space is divided in a number of small element for which linear equations can be assumed. Consequently, the system can then be represented by a large number of linear equations, which can be treated using matrix manipulation techniques. Image reconstruction will be dealt with in more detail in part 2.

## 3. SYSTEM DESCRIPTION

Figure 2 shows the main elements of the tomographic systems considered during this project. Several such systems have been designed and tested.

The system is split into three main sub-systems (sensor array, conditioning electronics and host computer). As described earlier, the sensor array is energised with an AC magnetic field created by one or more of the excitation coils. Electrically conductive or ferromagnetic objects within the space cause the distribution of the applied magnetic field to be modified and the resultant field changes are measured on the periphery of the space with an array of detection coils. These measurements are fed into a host computer. A set of measurements is taken for a variety of flux injection patterns. From the acquired data, the host computer is then able to produce an image of the material distribution by using suitable reconstruction software, which is shown in a much simplified form in the diagram as a matrix multiplication converting measured data values to pixel values.

during calibration. Large, high frequency, soft magnetic components present some production difficulties and a number of fabrication techniques have been tried. Bonded ferrite powder / polymer composites have, to date, proved to be the most practical solution, for example, an epoxy / manganese zinc composite ( $\mu_R = 14$ ) was used on one sensor design.

The excitation coils and detection coils can be constructed by both manual wire winding and printed circuit board (PCB) methods. Experience has shown that the coils should to be designed for optimum performance at a particular operating frequency. It is difficult to obtain satisfactory coil performance for changes in excitation frequency, which are greater than a decade. Consequently multi-frequency techniques, which have been researched for EIT, may have significant implementation difficulties for EMT. The optimum number of turns for the coils is a compromise between maximising sensitivity, with as many turns

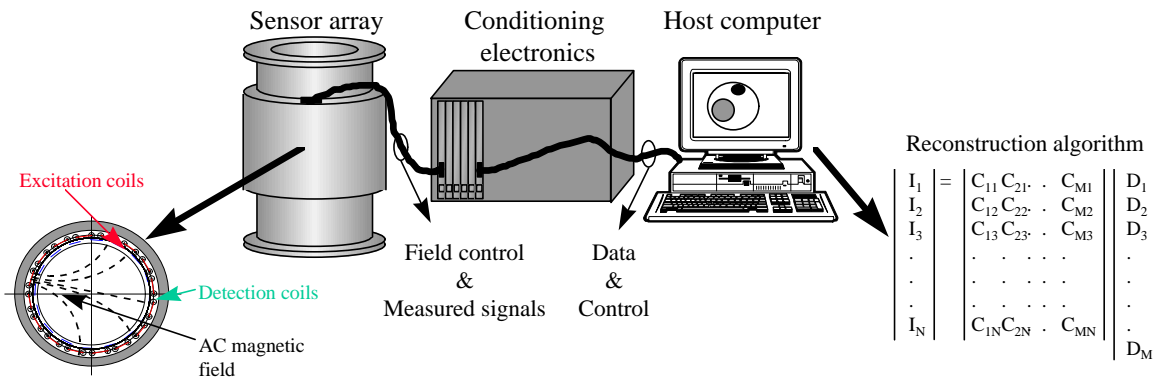


Figure 2: Block diagram of a typical EMT system

### 3.1. Sensor array

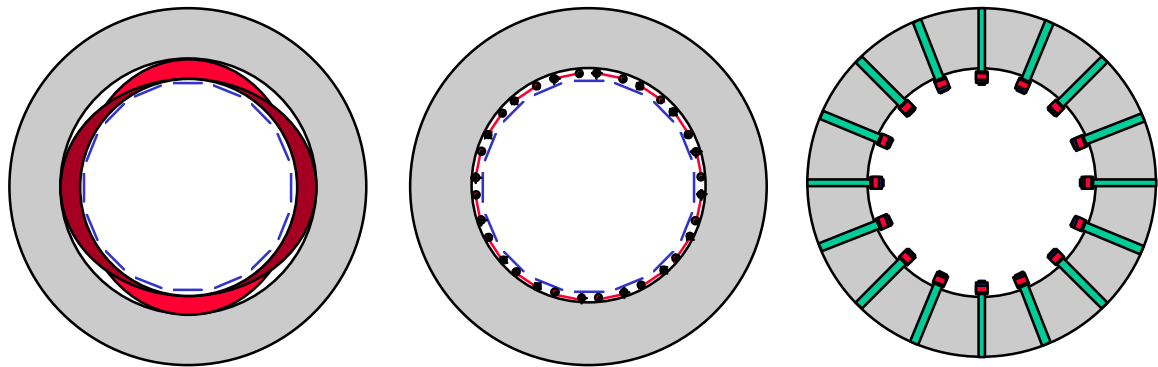
The sensor array is composed of:

- an outer magnetic confinement shield
- excitation coils
- detection coils
- current driver for each excitation coil
- buffer / amplifiers for detection coils.

The outer soft-magnetic screen performs several functions [6]. In particular, it confines the interrogating field within the sensor and avoids interference from external conductive or magnetic objects in the near vicinity. It also increases the sensitivity by a factor of up to two; and finally, reduces susceptibility to external magnetic interference by providing a shunt path around the object space. The screen can be omitted if all interfering objects in the near environment are fixed in position and their effects can be subtracted

as possible, and avoiding circuit resonance, which dictates the upper limit.

A number of coil geometries have been investigated as shown in Figure 3. The parallel design [4] has problems with the limited number of independent measurements. The multi-pole design uses ferrite concentrators to ensure as much flux as possible pass through each coil [7]. The planar coil approach can exploit nulls in mutual coupling between overlapped coils in order to minimise variations in the baseline signal [8]. Further innovative coil designs may offer some scope for improving future system performance especially gradiometers but this work beyond is the scope of the present study.



(a) Parallel design

Large excitation coils surround the object space. The coils have a sinusoidally distributed turns density. Limited independent measurements.

(b) Planar coils

Rectangular flat coils with excitation and detection coils overlapping each other in order to minimise the background coupling between adjacent coils.

(c) Ferrite cored

coils based on circular ferrite rods. Both excitation and detection coil(s) are mounted on the same pole.

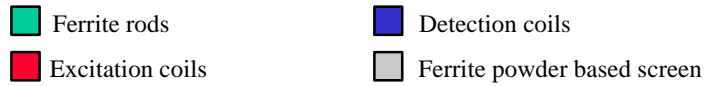


Figure 3: Summary of sensor array designs

### 3.2. Conditioning electronics

The conditioning electronics has purposely been designed in a modular format for flexibility as shown in a simplified form in Figure 4 for each excitation channel and detection channel respectively.

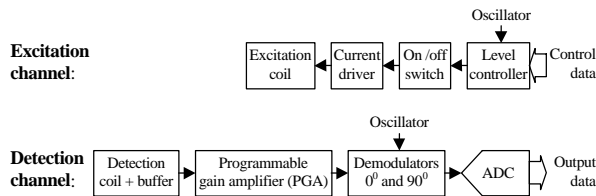


Figure 4: Simplified block diagram of a channel

The excitation channel contains a level controller, which sets the amplitude and phase (either  $0^\circ$  or  $180^\circ$ ) on a linear scale with  $2^{12}$  possible levels between +10V (i.e. 10 V amplitude,  $0^\circ$  phase), through 0 V, to -10 V (i.e. 10 V amplitude,  $180^\circ$  phase). Several options were considered and tested for the level controller, including CMOS R-2R ladder DAC's, bipolar multiplying DAC's, digital potentiometers, and even custom circuitry. A 12 bit DAC and an analogue multiplier eventually proved to be the most appropriate solution. The on / off switch is included to ensure an accurate zero value which is free from DAC and multiplier offset drifts.

The detection circuitry consists of a programmable gain amplifier (PGA) with gain steps of 1 to 512 (i.e. 29) in ten binary steps (i.e. 1, 2, 4, etc., 512) and a bandwidth well in excess of 1 MHz on all gain ranges. The demodulator has been designed using

two precision analogue multipliers (AD734 based) to derive the  $0^\circ$  and  $90^\circ$  components respectively. This module provides demodulation for a set of 16 input signals. Parallel multiplying demodulation is performed with respect to both  $\sin(\omega t)$  and  $\cos(\omega t)$  producing the in-phase ( $0^\circ$ ) and quadrature ( $90^\circ$ ) components. The demodulator's outputs, via suitable low pass filtering, can be written as:

$$\bar{V}_{In-Phase} = \frac{V_{Input} * V_{Real-Ref}}{10} = \frac{K \sin(\omega t + d) * 10 \sin(\omega t)}{10} \equiv \frac{K \cos(d)}{2} \Big|_{LPF: \omega_c \ll \omega} \quad (2)$$

$$\bar{V}_{Quadrature} = \frac{V_{Input} * V_{Im-ag-Ref}}{10} = \frac{K \sin(\omega t + d) * 10 \cos(\omega t)}{10} \equiv \frac{K \sin(d)}{2} \Big|_{LPF: \omega_c \ll \omega} \quad (3)$$

Each multiplier is followed by a 3rd order Butterworth low pass filter with a 3 dB cut-off frequency,  $f_c$ , at 5 kHz to extract the DC component. The bandwidth of the filters is critical to the system performance as it defines key system performance parameters such as dynamic performance and the effective noise bandwidth of the system [9]. For  $f_c = 5$  kHz, the settling time for a particular excitation profile is approximately 600  $\mu s$ , which for 16 excitation profiles per frame defines a maximum image capture rate of 100 frames/s. The DC components are finally fed to a 12 bit ADC.

Figure 5 shows the main blocks in the control of each excitation element. As can be seen, the channels are repeated 16 times and common functions are contained on the same circuit board.

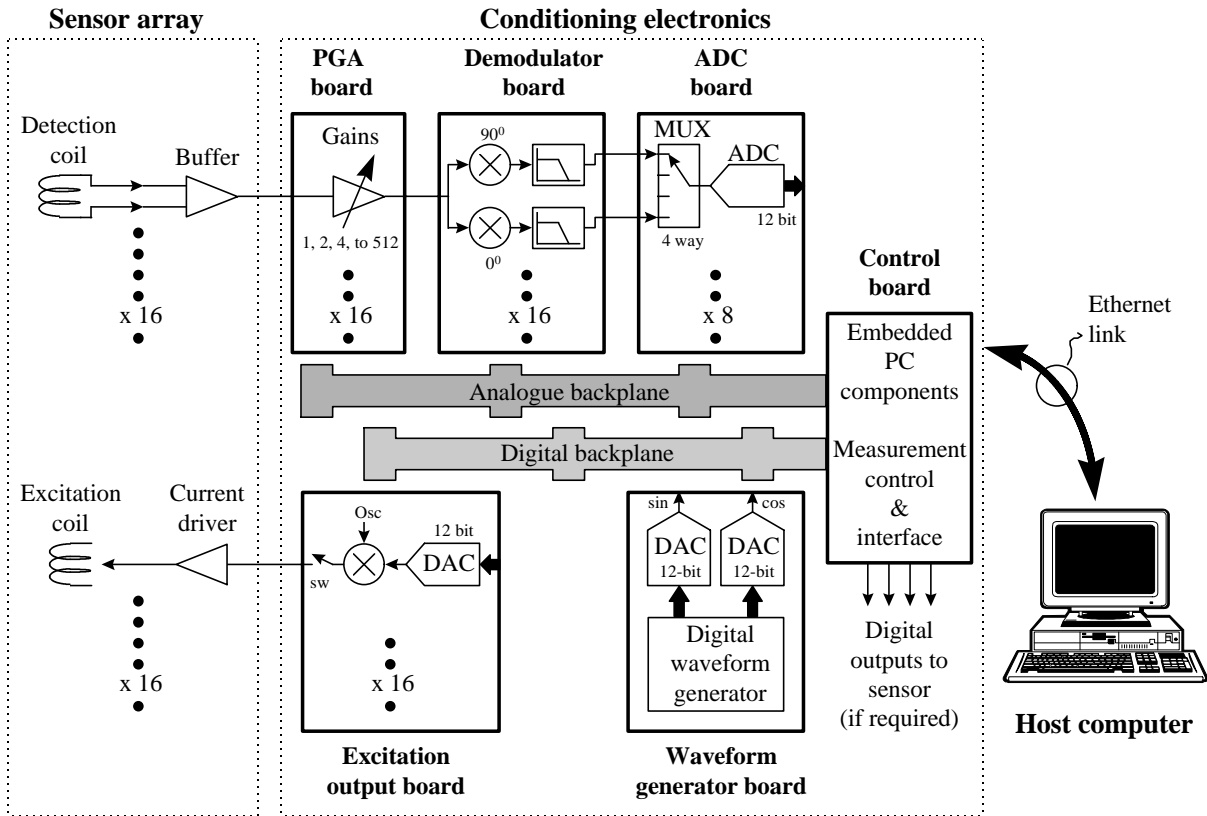


Figure 5: System block diagram

The conditioning electronics is housed in a standard 6U high Eurocard case. The various cards in the previous block are connected together by a 64 way analogue backplane and a 96 way digital backplane. In addition some of the more critical analogue signals were connected directly between boards internally. The system can be controlled by an embedded PC, which communicates to the host via an ethernet link. This enables the host computer to be positioned remotely.

The following table lists the time requirements associated with the main operations performed by the latest embedded PC controller.

Task	Time ( $\mu$ s)
Filter settling time for each projection (16 @ 600 $\mu$ s per projection)	9,600
ADC conversion time (16 @ 50 $\mu$ s per projection)	800
Load first projection	180
Read last conversion	280
Copy data into message	500
Send message to ethernet controller	400
<b>Total</b>	<b>11,760</b>

Table 2: Frame capture rates

The maximum frame capture rate can be increased either by decreasing the filter settling times or by taking less measurements per frame. The EMT system acquires a total of 512 measurements (i.e. 2 components at 0° and 90°, 16-detector coils, and 16 excitation projections)

#### 4. SENSOR SIMULATION

Finite element (FE) simulation [10] proved to be a very effective tool for studying EMT systems and Maxwell 2D (Ansoft Corp. USA) was extensively used during this work. A variety of fundamental issues were addressed in this manner and some examples are covered in the following sub-sections:

##### 4.1. Simulated sensitivity maps

A sensitivity map is the x, y response of a particular detector element to the position of a small perturbation in object material properties, under defined excitation conditions. The perturbation is swept over the entire object space to produce the map. In this study, the sensitivity maps were obtained by using a small circular target object of 10 mm diameter to represent the perturbation (which is typically  $\frac{1}{15}$  to  $\frac{1}{20}$  of object space diameter). Only perturbations with respect to empty

space were considered and the target object was taken either to be ferrite, copper or aluminium. The empty space value under identical excitation conditions was subtracted from the outputs of the detector coil. In order to reduce computational time only a limited number of object positions were simulated and interpolation was then used. This procedure consisted of angular, followed by radial interpolation using a cubic spline and the angular and radial interpolation was then repeated once more to further fill the gaps. Figure 6 shows a typical example of simulated sensitivity map for a ferrite test object; with coil 0 energised and coil 3 as the detector. Note the two equal positive peaks adjacent to coil 0 and coil 3 positions.

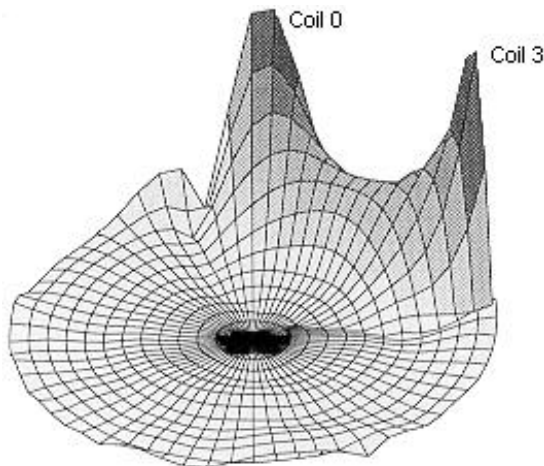


Figure 6: Example of a simulated sensitivity map

#### 4.2. FE simulation as a tool for reconstruction algorithm research

Sensitivity maps are an essential part of some reconstruction algorithms. The data from a complete set of sensitivity maps can be organised into a single 2 dimensional matrix which describes the response of the system to every pixel, for every detection coil, with every excitation coil energised in turn. This matrix characterises the system and is termed the projection matrix. It is a vital part of many of the reconstruction processes studied in this research project. Reconstruction algorithms based on simulated data or employing a simulated projection matrix were tested or optimised using simulated input data. This enabled routines and operations within the reconstruction process to be studied free from hardware related errors and with input data and projection matrices that were known to closely resemble the real situation.

#### 4.3. Optimising the sensor array design

FE simulation was used to investigate key areas of sensor array design including the spatial and contrast resolution of the sensor array, comparisons of different coil designs and the effects of screening. In order to assess spatial

resolution, simulations were performed to determine the smallest objects that could be detected using a target shown in the Figure 7 containing 4 copper bars. Changes in detector signals for objects diameter,  $d$ , down to 10 mm (i.e. 7 % of object space diameter) could readily be resolved by the simulator. Quantisation noise in the simulations prevented smaller objects from being studied. Simulations were also performed to assess the range of relative permeability and electrical conductivity that could be detected for a small object (diameter 15 mm, ~10% object space diameter) placed in the centre in order to assess contrast resolution.

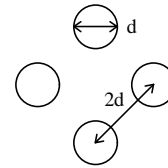


Figure 7: Target used for assessing spatial resolution

As a final example, the screen performs several different functions and there are a number of different approaches to its fabrication. Ferrite powder and bonded powder offer very cost effective solutions for realising this key component, however, these materials have relatively low magnetic permeabilities and consequently wider screens are needed than would be the case for a typical solid ferrite. The design trade-offs have been simulated [6], and as an example of this work, Figure 8 shows the trade-off between screen thickness, relative permeability and relative field strength for the parallel EMT sensor in [4]. From this graph, a screen thickness of 25 mm and a relative permeability of 15 were chosen.

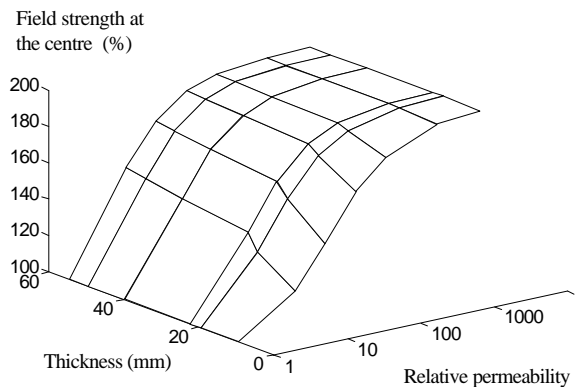


Figure 8: Ferrite screen design trade-offs

## 5. CONCLUSIONS

In conclusion, this paper has addressed most of the key issues in understanding how to develop EMT hardware and what are the performance limitations of these instruments. The research has

clearly shown the viability of the technique at the fundamental stage of research and substantial foundations have been laid for future applied industrial research on intelligent inductive sensor systems for tomographic imaging and inspection.

## ACKNOWLEDGEMENTS

This work was supported by the European Community through the Brite EuRam programme, project number BE-7961-93, and contract number BRE2-CT94-0604.

## REFERENCES

- [1] R.A. Williams and M.S. Beck (ed.'s), "*Process Tomography: Principles, Techniques and Applications*" ISBN 0 7506 0744 0, Butterworth Heinemann, 1995.
- [2] Z.Z. Yu, A.J. Peyton, W.F. Conway, L.A. Xu and M.S. Beck, "*Imaging system based on electromagnetic tomography (EMT)*", Electronics Letters, **29**(7), pp. 625-26, 1993.
- [3] S. Al-Zeibak and N.H. Saunders, "*A feasibility study of In Vivo electromagnetic imaging*", Phys. Med. Biol., **38**, pp. 151-60, 1993.
- [4] Z.Z. Yu, A.J. Peyton, L.A. Xu and M.S. Beck, "*Electromagnetic inductance tomography (EMT): sensor, electronics and image reconstruction for a system with a rotatable parallel excitation field*", IEE Proc. Sci. Meas. Technol., **145**(1), pp. 20-25, 1998.
- [5] A.J. Peyton, Z.Z. Yu, G.M. Lyon, S. Al-Zeibak, J. Ferreira, J. Velez, F. Linhares, A.R. Borges, H.L. Xiong, N.H. Saunders and M.S. Beck, "*An overview of electromagnetic inductance tomography: description of three different systems*", Meas. Sci. Technol., **7**, pp. 261-271, 1996.
- [6] Z.Z. Yu, P.F. Worthington, S. Stone and A.J. Peyton, "*Electromagnetic screening of inductive tomography sensors*", European Concerted Action on Process Tomography conference, Bergen, Norway, ISBN 0 9523165 2 8, pp. 300-10, 1995.
- [7] J. Ferreira, F. Linhares, J. Velez, J. E. de Oliveira, and A.R. Borges, "*Imaging of conductive and ferromagnetic materials using a magnetic induction technique*", 12th annual review of progress in Applied Computational Electromagnetics, pp. 367-374, Monterey Ca. USA, 1996.
- [8] P.B. Roemer, W.A. Edelstein, C.E. Hayes, S.P. Souza, and O.M. Mueller, "*The NMR phased array*", Mag. Resonance in Med., **16**, pp. 192-225, 1990.
- [9] R.W.M. Smith, I.L. Freeston, B.H. Brown, and A.M. Sinton, "*Design of a phase-sensitive detector to maximise signal-to-noise ratio in the presence of Gaussian wideband noise*" Meas. Sci. Technol., **3**, pp. 1054-1062, 1992.
- [10] P.P. Silvester and R.L. Ferrari, "Finite elements for electrical engineers" 3rd edition Cambridge University Press, ISBN 0 521 44505, 1996.